Mg^{2+} modulates the activity of hyperpolarization-activated calcium currents in plant cells

Fouad Lemtiri-Chlieh[1,2], Stefan T. Arold[1,3,4] and Chris Gehring[1,5]

1: King Abdullah University of Science and Technology (KAUST), Biological and Environmental Science and Engineering (BESE), Thuwal, 23955-6900, Saudi Arabia.
2: Department of Neuroscience, University of Connecticut School of Medicine, Farmington, CT 06030
3: King Abdullah University of Science and Technology (KAUST), Computational Bioscience Research Center (CBRC), Thuwal, 23955-6900, Saudi Arabia.
4: Centre de Biochimie Structurale, CNRS, INSERM, Université de Montpellier, 34090 Montpellier, France
5: Department of Chemistry, Biology & Biotechnology, University of Perugia, ITALY

Running Title: *Mg^{2+} regulates HACC in plants*

To whom correspondence should be addressed: Fouad Lemtiri-Chlieh, flemtiri@gmail.com

Keywords: hyperpolarization-activated calcium channels, HACCs, cyclic nucleotides-activated channels, CNGCs, Magnesium, guard cells, patch clamp

---

ABSTRACT

Hyperpolarization-activated calcium channels (HACCs) are found in the plasma membrane and tonoplast of many plant cell types where they have an important role in Ca^{2+}-dependent signaling. The unusual gating properties of HACCs in plants, i.e., activation by membrane hyperpolarization rather than depolarization, dictates that HACCs are normally open at physiological hyperpolarized resting membrane potentials (the so called pump or P-state), thus, if not regulated, they would be continuously leaking Ca^{2+} into cells. In guard cells, HACCs are permeable to Ca^{2+}, Ba^{2+} and Mg^{2+}, activated by H_2O_2 and the plant hormone abscisic acid (ABA) and their activity is greatly reduced by low amounts of free cytosolic Ca^{2+} ($[Ca^{2+}]_{Cyt}$) and hence will close during $[Ca^{2+}]_{Cyt}$ surges. Here we demonstrate that the presence of the commonly used Mg-ATP inside the cell greatly reduces HACC activity especially at voltages $\leq$ -200 mV and that Mg^{2+} causes this block. We therefore conclude, firstly, that physiological cytosolic Mg^{2+} levels affect HACCs gating and that channel opening requires either high negative voltages ($\geq$ -200 mV) and/or displacement of Mg^{2+} away from the immediate vicinity of the channel. Secondly, based on structural comparisons with Mg^{2+}-sensitive animal inward-rectifying K^+ channel, we propose that the likely candidate HACCS described here are cyclic nucleotide gated channels (CNGCs), many of which also contain a conserved di-acidic Mg^{2+}-binding motif within their pores. This conclusion is consistent with the electrophysiological data. Finally, we propose that Mg^{2+}, much like in animal cells, is an important component in Ca^{2+} signalling and homeostasis in plants.

INTRODUCTION

Ca^{2+} has long been recognized as an essential component in many plant cellular processes and in order for Ca^{2+} to function as an intracellular signal, temporal, spatial and stimulus specific changes in $[Ca^{2+}]_{Cyt}$ need to be tightly controlled (1). Ca^{2+}-influx into plant cells is achieved, at least in parts, by three main types of Ca^{2+}-channels (2,3): Firstly, channels that show little or no voltage sensitivity, referred to as non-selective

calcium channels (NSCCs) primarily for being active at all voltages and for being less selective for calcium over monovalent cations such as K^+ and Na^+ (4); secondly, channels that show high voltage-dependence like those activated by depolarization (DACCs) (5) and thirdly others, which are the focus of this report, activated only by membrane hyperpolarization (HACCs) (6).

In guard cells, Ca^{2+} was shown to be involved in abscisic acid (ABA) signaling and stomatal guard cell movements (7,8) and using the patch clamp technique in both whole cell (WC) and excised configurations (EC), two types of HACCs were identified at the plasma membrane (PM). One type of HACCs is highly selective for Ca^{2+} (over K^+ and Cl^-) (9). Its activity is enhanced by ABA (9,10), H_2O_2 (10), and by external Ca^{2+} itself, an apparently unique property of this particular plant HACC (11). Meanwhile, increasing $[Ca^{2+}]_{Cyt}$ from 0.2 to 2 μM decreased the open probability (P_o) of this HACC by a factor of 10 (9), implying a critical role of $[Ca^{2+}]_{Cyt}$ in the feedback regulation of the channel. The proteins responsible for this type of channel have not being identified to-date. This is not the case for the other type of HACCs where a family of 20 genes is known and their translation products were originally described as being mostly gated open by cyclic nucleotides such as 3',5'-cyclic adenosine monophosphate (cAMP) or 3',5'- cyclic guanosine monophate (cGMP) (12), hence their name: cyclic nucleotide gated channels (or CNGCs). Moreover, these plant channels, like their animal functional homologs, poorly discriminate between divalent and monovalent cations. Indeed, when heterologously expressed in oocytes, these channels are not only permeable to Ca^{2+} (13) but found to be equally permeable to monovalent cations such as K^+, Rb^+, Na^+, Li^+ and Cs^+ (13,14). Similar inwardly-rectifying currents permeable to either Ca^{2+}, Ba^{2+} and even Na^+, activated by cAMP (15) and cGMP (16) were also characterized in guard cells with the patch clamp technique. The latter work demonstrated that the highly expressed CNGC5 and CNGC6 genes in guard cells are directly responsible for the recorded HACC activity. Likewise, in pollen tubes of Asian pear tree (*Pyrus pyrifolia* Nakai cv. Hosui), a HACC that conducts indiscriminately either Ca^{2+} or K^+ was shown to be activated by cAMP and down regulated by high $[Ca^{2+}]_{Cyt}$ (17). It is noteworthy that all these type-two HACCs share one common characteristic, they are sensitive to low concentrations of Lanthanides (10,15-17).

We know from previous work, particularly in animal systems, that Mg^{2+} ions are key regulators of many ion channels and receptors (18). For instance, the inwardly rectifying K^+ (Kir) channels and TRPV6, a member belonging to a subgroup of transient receptor potential (TRP) cation channels, both show strong Mg^{2+}-dependent gating (19,20). Another example of a voltage-dependent block by Mg^{2+} ions is the N-methyl-D-aspartate (NMDA) receptor (21,22); in this case extracellular Mg^{2+} is responsible for this effect. By contrast, in plants, the rectification of $I_{K,in}$ was found not to be due to a Mg^{2+}-dependent block (23) but rather to an intrinsic property of the channel protein itself (24). However, ion channels localized to the tonoplast with a key role in stomatal volume regulation, such as the slow- (SV) and the fast- (FV) activating vacuolar channels, were shown to be affected by cytosolic Mg^{2+} ions (25-28). Indeed, it was found that, besides Ca^{2+}, Mg^{2+} also promoted the activation of SV channels affecting their kinetics (time constants of channel activation and de-activation) and voltage-dependent activation characteristics. At the same time, Mg^{2+} inhibits FV channels, thus reducing K^+ leakage from the tonoplast (25). Mg^{2+} was also shown to inhibit an outward NSCC, termed MgC, which was characterized in the PM of guard and subsidiary cells of *Vicia faba* and *Zea mays* (29). Another NSCC example from N_2-fixing plants where Mg^{2+} plays a critical role is related to the transport of ammonium (NH_4^+)/ammonia (NH_3) across the peribacteroid membrane (30). This is achieved in part through a passive non-selective electrogenic transport system, regulated by Ca^{2+}, but more recently, this channel was described as having 'unusual' characteristics such as an inward rectification caused by Mg^{2+} on the cytosolic face and a very low single channel conductance (< 0.2 pS with 150 mM KCl + 10 mM $CaCl_2$ in the pipette and 150 mM NH_4^+ in the bath) which was found to be inhibited by Mg^{2+} from the luminal face of the symbiosome (31).

ATP is another major regulator of ion channel gating. One of the best characterized channels is the K_{ATP}, an inward K^+-rectifier (from the K_{ir} family of genes) found mostly in cardiac and skeletal muscles, neurons and pancreatic β-cells (18). These channels are normally closed in the presence of ATP and only open, to hyperpolarize the cell membrane, when cytosolic ATP levels drop. ADP added in the form of Mg-ADP can restore the activity of K_{ATP} that were pre-treated with ATP (32,33). In guard cells, Mg-ATP is required for blue light-activated outward currents (34). Indeed, it was found that 1 to 2 mM Mg-ATP, as well as other intracellular substrates, are required to fully activate a plasma membrane electrogenic ion pump capable of hyperpolarizing the membrane to around -140 mV, a potential well beyond the activation threshold for $I_{K,in}$ (35).

Given the importance and the key role that calcium channels play in plant cellular signaling including guard cell aperture regulation, we address the question of whether internal Mg^{2+} can affect HACCs activity in guard cell protoplasts (GCPs) and show examples of the Gd^{3+}-sensitive Ba^{2+}-currents (I_{Ba}) activated by hyperpolarization with and without Mg^{2+} in the patch pipet. We also assess important properties of I_{Ba} in the absence of Mg^{2+} such as the permeability and sensitivity to some relevant inorganic compounds and physiological effectors such as abscisic acid (ABA) and cAMP.

EXPERIMENTAL PROCEDURES

Protoplast isolation - *Vicia faba* L. *cv* (Bunyan) Bunyan Exhibition seeds were grown on vermiculite under conditions described previously (36). *Arabidopsis thaliana* (Columbia) seeds were grown on peat pellets (jiffy, Oslo) in a controlled environment growth chamber (Percival, CLF plant climatic, Wertingen) at 22 °C on a 8/16-h light/dark cycle. Guard cell protoplasts (GCPs) were isolated from either 3- to 4- week *V. faba* or 5- to 6- week *A. thaliana* plants. GCPs were isolated from abaxial epidermal strips as described previously (37). Briefly, epidermal strips were floated on medium containing 1.8-2.5% (w/v) Cellulase Onozuka RS (Yacult Honsha, Tokyo, Japan), 1.7-2% (w/v) Cellulysin (Calbiochem, Behring Diagnostics, La Jolla, CA), 0.026 % (w/v) Pectolyase Y-23, 0.26 % (w/v) BSA, and 1 mM $CaCl_2$ (pH 5.6) with osmolality adjusted with sorbitol to 360 $mOsm.kg^{-1}$. After 90-120 min incubation in the dark at 28 °C with gentle shaking, released protoplasts were passed through a 30 µm mesh, and kept on ice for 2 to 3 min before centrifugation (100 g for 4 min at room temperature). The pellet consisting of GCPs was re-suspended and kept on ice in 1 or 2 ml of fresh medium containing 0.42 M mannitol, 10 mM 2-(N-morpholino)ethanesulfonic acid (Mes), 200 µM $CaCl_2$, 2.5 mM KOH (pH 5.55 and osmolality at 466 $mOsm.kg^{-1}$). Unless stated otherwise, all chemicals were from Sigma (Sigma-Aldrich Co. St Louis, MO).

Solutions - Protoplasts were placed in a 0.5 ml chamber, left to settle down, and then perfused continuously at flow rate of ≈ 0.5-1 ml/min. To record I_{Ba} currents through HACC, we used barium containing solutions. The bath medium contained (in mM): 100 $BaCl_2$, 10 Mes (pH 5.5 with Tris base) and the pipette contained (in mM): 100 $BaCl_2$, 4 EGTA, 10 Hepes (pH 7.5 with Tris). Experiments where $I_{K,in}$ and I_{Ba} measurements were made on the same GCPs a different bath and internal solutions as follows. Bath (in mM): 30 KCl, 10 Mes (pH 5.5 with Tris base) to measure $I_{K,in}$ and was replaced by 100 $BaCl_2$, 10 Mes (pH 5.5 with Tris base) to measure I_{Ba}. Internal solution (in mM): 1 $BaCl_2$, 18 KCl, 4 EGTA, 10 Hepes (pH 7.5 with Tris base). Mg-ATP, $MgCl_2$ and/or K_2-ATP were added as specified in the figures. Osmolality was adjusted with Sorbitol to 210$mOsm.kg^{-1}$. For classic solutions used to measure $I_{K,in}$ (Fig. 4 A, and B), refer to (38). ABA was added externally. All chemicals were from Sigma Chemical, Poole Dorset, UK. The membrane permeable cAMP analog Bt_2cAMP was solubilized in deionized water and stored in aliquots of 50–100 µl at a concentration of 0.1 M. Bt2cAMP was diluted to the final desired concentration just a few minutes before its use.

Current-voltage recording and analysis - Patch pipettes (5-10) were pulled from Kimax-51 glass capillaries (Kimble 34500; Kimble, Owens-Illinois) using a two stage puller (Narishige PP-83, Japan). Experiments were performed at room temperature (20 to 22 ^oC) using standard whole-cell patch clamp techniques, with an Axopatch 200B Integrating Patch Clamp amplifier (Axon Instruments, Inc. Union City, CA, U.S.A.). Voltage commands and simultaneous signal recordings and analyses were assessed by a microcomputer

connected to the amplifier via multipurpose Input/output device (Digidata 1320A) using pClamp software (versions 8.0 and 10; Axon Instruments, Inc.). After Giga-Ohm seals are formed, the whole-cell configuration was then achieved by gentle suction, and the membrane was immediately clamped to a holding voltage (h_v) of -36 mV. GCPs were continuously perfused throughout the experiment and current recordings began only after at least 5-10 min from going into whole-cell mode to allow for intracellular equilibrium between cytoplasm and patch pipet solution. All current traces shown were low-pass filtered at 2 kHz before analog-to-digital conversion and were uncorrected for leakage current or capacitive transients. Membrane potentials were corrected for liquid junction potential as described (39). Ionic activities were calculated using GEOCHEM-EZ (40). Current-voltage (I-V) relationships for I_{Ba} and $I_{K,in}$ were plotted as steady-state currents *vs.* test potentials when using the square pulse stimulations or utilizing the "Trace *vs* Trace" feature of Clampfit analysis when using voltage ramps. Unless otherwise stated, every experiment reported here was repeated a minimum of three times and data were graphed as mean±s.e.m.

Homology modeling - Models were built using Swiss Model and structures visualized with PyMOL (The PyMOL Molecular Graphics System, Version 1.5.0.4 Schrödinger, LLC). Multi-sequence alignments were produced with Muscle (43).

RESULTS

Removal of intracellular Mg-ATP unveils a larger instantaneously-activated, inwardly-directed and Gd^{3+}-sensitive Ba^{2+}-current. - We recorded Ba^{2+}-currents (I_{Ba}) in guard cell protoplasts either in the presence or absence of Mg-ATP (Fig. 1A) and at the end of the trials we also tested for I_{Ba} sensitivity to Gd^{3+}, a potent blocker of I_{Ba} (Fig. 1B). The recorded currents were generated in response to a square pulse protocol from +64 mV to -256 mV in increments of -20 mV with the holding voltage (h_V) set to -36 mV. In the presence of Mg-ATP (Fig.1 A; left panel), a small instantaneous inward-rectifying current of ≈ -20 pA started to activate around -200 mV to only reach a maximum of -60 pA at -256 mV. This current was, as expected, sensitive to the addition of extracellular Gd^{3+} (see Fig. 1B; left panel). Meanwhile in the absence of Mg-ATP (Fig. 1A; right panel), much larger (≥ 8-fold) instantaneous rectifying-currents, which happened to be also Gd^{3+}-sensitive were recorded (Fig. 1B; left traces). The current-voltage (I-V) relationships in the presence (●; n=3) or absence (○; n =7) of Mg-ATP are represented in Figure 1C (left panel). We also plotted the effect of Gd^{3+} on the I-V relationships in the presence (■) or absence (□) of Mg-ATP (Fig. 1C; right panel). These results highlight that when omitting Mg-ATP from the intracellular medium, a larger Gd^{3+}-sensitive inwardly-rectifying Ba^{2+}-current is unveiled that activates at significantly less negative voltages (see the shift to the right of ≥ -100 mV in the I-V plot). Furthermore, the currents recorded in 0 Mg-ATP seem to reverse near the calculated Nernst equilibrium potential for Ba^{2+} (E_{Ba} ≈ +28 mV), and are far removed from E_{Cl} (-54 mV). Likewise, using fast depolarization ramps (0.07 V/sec) after activating the current I_{Ba} with a square pulse to -156 mV (see voltage protocol and current trajectories in Fig. 1D; left), a reversal potential of +17 mV was measured, again close to E_{Ba} rather than E_{Cl} (see Fig. 1D, zoomed I-V plot). This is also indicative of the higher permeability of this conductance to Ba^{2+} as compared to Cl^-.

To test whether changing external Ba^{2+} concentration will affect current magnitude as well as the I-V relationship, GCPs were patched in whole cell mode using the Mg-ATP free internal solution (Fig. 2). Once again, the current magnitudes recorded in the absence of Mg-ATP are quite substantial. For instance, at -196 mV, a -280 pA current is measured in 100 mM $[Ba^{2+}]_{out}$ (Fig. 2A) while in 30 mM $[Ba^{2+}]_{out}$ (Fig. 2B) the same voltage gives rise to a current value of -220 pA. All current magnitudes at any given voltage are decreased when switching to lower $[Ba^{2+}]$ in the bath. The corresponding I-V plots appear as shifting to negative values (Fig. 2C) when switching from 100 to 30 mM Ba^{2+} and this is accompanied by a negative shift in the apparent reversal potential (E_{rev}) values. Indeed, when zooming in (Fig. 2C, inset), the apparent E_{rev} shows a negative shift of ≈ -14 mV as a result of this Ba^{2+} concentration change. Furthermore, the

apparent E_{rev} in 30 mM $[Ba^{2+}]_{out}$ (≈ +8 mV) is still closer to the calculated E_{Ba} rather than E_{Cl} which are in this case +17.7 mV and -25.7 mV respectively. This experiment was repeated with 100, 30 and 10 mM $BaCl_2$ in the bath and the same qualitative effects were seen i.e., decrease of current amplitude when decreasing the [Ba2+]$_o$ and negative shift in the apparent E_{rev} (data not shown).

HACC permeability sequence to divalent cations in the absence of Mg-ATP: Ba > Ca ≈ Sr ≈ Mn >> Mg.- Guard cell permeability to other divalent cations such as Ca^{2+}, Sr^{2+}, Mn^{2+} and Mg^{2+} in the absence of Mg-ATP was also tested (Fig. 3). As expected, HACC was permeable to Ca^{2+} (Fig. 3A) and found to have similar permeability to both Sr^{2+} (Fig. 3A) and Mn^{2+} (Fig. 3B). Meanwhile Mg^{2+} did not permeate HACC (Fig. 3A). The I-V plots (Fig. 3A and B) summarizes the permeability data: i.e., the lack of HACC permeability to Mg^{2+} as well as the much larger permeability to Ba^{2+} when compared to either Ca^{2+}, Sr^{2+} or Mn^{2+}. The effect of Mn^{2+} ions over time is reported in Figure 3B and highlights the unique behavior of this ion. Unlike Ca^{2+} or Sr^{2+}, Mn^{2+} (Fig. 3B) triggered a transient block of HACC followed by some current recovery while still washing out the Ba^{2+} and replacing it with 100 mM Mn^{2+}. This transient block effect was repeated on two other GCPs but was never seen with either Ca^{2+} or Sr^{2+}; nor was it seen with Mg^{2+} even after 20 minutes of washing out Ba^{2+}.

HACC permeability sequence to monovalent cations in the absence of Mg-ATP: K≈*Na>Ba>Cs>>TEA.*- We observed that this Gd^{3+}-sensitive HACC is also permeable to some physiologically relevant monovalent cations such K^+ (Suppl. Fig. 1A), Na^+ (Suppl. Fig. 1B) and Cs^+ (Suppl. Fig. 1C) but not tetraethylammonium (TEA^+)(Suppl. Fig. 1D). These data indicate that the Gd^{3+}-sensitive current characterized in this work does not select for small mono or divalent cations (except for the case of Mg^{2+} and the bigger cation TEA^+). Chloride too does not seem to permeate through this HACC. Indeed, when 100 mM Cl^- was added at the same time as TEA^+ (see Suppl. Fig. 1D), no current could be detected, indicating that Cl^- is as impermeable as TEA^+. Qualitatively, the same effect was seen in all patched GCPs (n = 5 for K^+ and Na^+; n = 2 for Cs^+ and TEA^+).

Effect of blockers of I_{Ba} in the absence of Mg-ATP and comparison with the effect on $I_{K,in}$. - In order to further characterize this HACC, readily unmasked when Mg-ATP was omitted from the patch pipet, the effect of some classical blockers such as the lanthanides (La^{3+} and Gd^{3+}), Mn^{2+}, Cs^+ and TEA^+ were tested on I_{Ba} as well as on $I_{K,in,}$ (the other major conductance that activates upon hyperpolarization in guard cells). One of the most conspicuous effects lies in the potent effect of Gd^{3+} in blocking I_{Ba} (Fig. 4A) even when used at relatively low concentrations (20 to 100 µM) while the same concentrations of Gd^{3+} had no effect on $I_{K,in}$ (Fig. 4A). An even higher concentration of Gd^{3+} (500 µM) did not affect $I_{K,in}$ (data not shown). La^{3+} also blocked I_{Ba} measured in 0 Mg-ATP, but we found that much higher concentrations of La^{3+} (0.2 to 0.5 mM) are needed to achieve the same block as compared to Gd^{3+} (data not shown). Experimenting with cesium, a blocker of $I_{K,in}$, hardly any effect on I_{Ba} was registered (Fig. 4B). Even though Cs^+ was used at concentrations up to 1 mM, it had only a small effect, if any, on I_{Ba} while the tenth of this amount (0.1 mM) is sufficient to block a large proportion (≈ 80% or more) of $I_{K,in}$ (Fig. 4B). Furthermore, Mn^{2+} used at 2 mM inhibited HACC by ≈ 37% (at V = -196 mV) when the charge carrier (in this case Ba^{2+}) was still present in the bath (Fig. 4C). Increasing Mn^{2+} concentration to 10 mM shows that Mn^{2+} is not an efficient blocker of I_{Ba} as compared to Gd^{3+} or La^{3+} and 10 mM Mn^{2+} only causes an extra 20% I_{Ba} inhibition (see IV plot in Fig. 4C). Finally, 10 mM tetraethylammonium chloride (TEA), a concentration that was shown to block 70 to 80 % of $I_{K,in}$ in intact guard cells (44), had no effect whatsoever on I_{Ba} (Fig. 4D) measured in 0 Mg-ATP.

Rapid enhancement of I_{Ba} by ABA. - Given that in guard cells, a HACC was implicated downstream of ABA in stomatal movements, we tested whether ABA affects I_{Ba} activated in the absence of internal Mg-ATP. We patch clamped guard cells to measure I_{Ba} currents under baseline conditions, i.e., zero Mg-ATP inside and no added ABA outside (Fig. 5). After about 10 minutes, the time usually necessary to reach steady-state conditions, we switched the perfusion solution to the one containing 20 µM ABA. A rapid and pronounced increase of I_{Ba} currents is seen at all voltages between -100 and -200 mV (≥ 1.3 to 1.5 fold)

after only 5 minutes of ABA treatment (Fig. 5B) and a near doubling of the size of the I_{Ba} currents occurs at 10 minutes (Fig. 5, A and B). The enhancement of I_{Ba} in response to ABA, especially at 10 minutes, spans from -60 to -200 mV and also appears to shift the activation threshold of I_{Ba} (Fig. 5B) to the right. This suggests that ABA not only enhances calcium entry through HACC but can also mobilize calcium entry at less negative voltages.

Characterization of the effect of Mg^{2+} on I_{Ba} and I_{Kin}. - To answer whether internal Mg^{2+} alone causes the block of I_{Ba} when we add Mg-ATP, GCPs were patched either without Mg-ATP or without ATP but with added Mg^{2+} (as $MgCl_2$). Furthermore, and as a control for 'ion transport functionality' of the patched GCPs, we used conditions that allow measurements of not just I_{Ba}, but also to record $I_{K,in}$. The experiments were started in conditions allowing to probe for $I_{K,in}$ with KCl (30 mM) in the bath and this was then followed by replacing the KCl with a solution containing $BaCl_2$ (100 mM). This was done first in the absence of both intracellular Mg^{2+} and ATP (Fig. 6A) and then repeated on another batch of guard cells with internal medium containing 1 mM $MgCl_2$ but no ATP (Fig. 6B). Firstly, in zero Mg-ATP the only current that activated in response to hyperpolarization was I_{Ba} (Fig. 6A). $I_{K,in}$ could not be activated. Secondly, when only Mg^{2+} was included in the pipet solution (no ATP added), $I_{K,in}$ could now be activated in 30 mM K^+, however, when switching the bath from K^+- to Ba^{2+}-containing media, I_{Ba} currents vanished (Fig. 6C) indicating that including only Mg^{2+} in the patch pipet can cause the block of I_{Ba} at voltages where they are normally activated in 0 Mg-ATP.

Could cAMP activate HACC in guard cells despite the presence of intracellular Mg^{2+}? - We know from our own previous work (15) that cAMP activated a Gd^{3+}-sensitive HACC in guard cells while recording in Mg^{2+}- and ATP-free media (see also, Suppl. Fig. 2A) but since we now show that this conductance discriminates poorly between divalent and monovalent cations, a hallmark characteristic of all animal as well as plant cyclic nucleotides gated channels (CNGCs) (13,45), we sought to check if the Gd^{3+}-sensitive I_{Ba} is also gated by cAMP in conditions where intracellular Mg^{2+} is present and I_{Ba} is already blocked (Suppl. Fig. 2B). In the absence of db_2cAMP (the lipophilic permeable analog of cAMP), and as expected only a small background I_{Ba} current is seen (≤10 pA around -190 mV). After perfusing with db_2cAMP (1 mM), a substantial increase in I_{Ba} amplitude between voltages from around -30 to -190 mV was observed (>60 pA around -190 mV). Keeping db_2cAMP in the bath and adding Gd^{3+} (50 μM) resulted in a total block of the current (≤4 pA around -190 mV). This may indicate that GCPs harbor CNGCs that can be activated by cAMP despite the blocking effect by Mg^{2+}.

Identification of candidate Mg^{2+}-dependent cation channels. – Crystallographic and functional analyses of a strong inward-rectifier K^+ channel (Kir2.2) from chicken (46) showed that the rectification characteristic can be explained by Mg^{2+}-binding to negatively charged regions in the pore (formed by D173) with possible additional contributions from acidic residues within the cytoplasmic regulatory domains (D256 and E300/E225) (Suppl. Fig. 3). To explore the possibility that a similar mechanism allows Mg^{2+} inward rectification for a subset of candidate plant channels that display the electrophysiological properties described here (i.e. activation by hyperpolarization and cAMP, absence of cation selectivity and inhibition by lanthanides), we built homology models of the pore-forming residues for AtCNGCs (47). The models were built using structures of the human hyperpolarization-activated channels HCN1, based on a ~22 % sequence identity. The obtained models clearly showed that AtCNGCs do not have a Mg^{2+}-binding site corresponding to the location of Kir2.2 D173 inside the pore region (Fig. 7A, left arrow, and Suppl. Fig. 3). However, a tandem glutamic acid motif that could form a possible di-acidic Mg^{2+}-binding site is found in most AtCNGCs located a little downstream of the pore in the so-called C-linker disc (Fig. 7). Akin to Kir2.2 D173 and E300/E225, this di-acidic AtGNCG motif forms a positively charged opening with distances of 7.3–8.3Å between neighbouring charges and a diameter of ~11Å [for Kir2.2 D173 these values are 7.3–7.4Å and 10.4–11.8Å, respectively (PDB 3jyc)]. As in Kir2.2, these distances between carboxyl groups are too large for a direct ion coordination, suggesting that Mg^{2+} is bound through bridging water molecules (46). Interestingly, this di-acidic motif is not present in AtGNCG2, which has been shown to be

an atypical family member with respect to ion selectivity (49). The di-acidic motif is also absent in HCN1, for which Mg^{2+} inward rectification has not been documented (Fig. 7C).

DISCUSSION

In order to record ion-currents (for instance $I_{K,in}$ or $I_{K,out}$) from plant cells in the "whole-cell" patch configuration, it is standard, for reasons highlighted in the introduction (see also: "Methods" section in (50)), to include ATP and Mg^{2+} either in the form of [Mg-ATP] or [$MgCl_2$ + K_2-ATP]. In contrast, the composition of the internal solution used to characterize the hyperpolarization-activated Ca^{2+}-current (HACC or I_{Ba}) is more variable especially with regards to ATP and Mg^{2+}. One notices for instance that ATP and Mg^{2+} are either both included (9,11,17,51,52) or completely omitted from the internal solution (10,16,53-55). Here, we carefully addressed the role and consequences of Mg^{2+} inclusion, either in the form of Mg-ATP or $MgCl_2$. We report experiments designed to assess the effect of Mg^{2+} on I_{Ba} current activated by hyperpolarization in GCPs, being aware that other cell types,, e.g., root cells, might indeed show different responses. We show that omitting Mg-ATP unmasked the presence of an instantaneously-activating inwardly-rectifying conductance. This 'newly unveiled' conductance still retains most of the biophysical and pharmacological characteristics that are hallmarks of the classical I_{Ca}-type (9,10) and CNGCs which we referred to here as either I_{Ba} or HACCs (13,14). Like $I_{K,in}$, this conductance is activated by hyperpolarizing-going voltages and shows some voltage-dependent rectification (but not as strongly as compared to $I_{K,in}$ for instance; see Fig. 4A). Also, typical of HACCs, we found that besides Ba^{2+}, other divalent cations such as Ca^{2+}, Sr^{2+} and Mn^{2+} also permeate this channel but at a much slower rate than Ba^{2+} does, hence the smaller currents resolved even though using the same amounts of divalent cations in the bath. More importantly, this HACC is activated by cAMP as well as permeable to monovalent cations (see Suppl. Fig. 1 and 2), which are definite attributes of CNGCs. HACCs including CNGCs are specifically blocked by low concentrations of extracellular Gd^{3+} that are far less effective in blocking $I_{K,in}$ (see Fig. 4A). Equally important, we found that the unmasked I_{Ba} is also enhanced by ≈ 1.3- to 1.5-fold in response to 5 minutes treatment with ABA and up to 2-fold after 10 minutes. Similarly, it was shown that ABA increases a PM I_{Ca}-type whole-cell current in *Arabidopsis* guard cells by ≈ 2- to 3-fold within 5 minutes of treatment (9). Note that the ABA effect reported here was obtained not only in Mg^{2+}-free but even more importantly in ATP-free internal solution, thus indicating that ATP is not as crucial for this channel as was suggested by an earlier report (56). This is, in fact, in agreement with many other reports showing that indeed ABA can increase cytosolic Ca^{2+} levels through activation of PM calcium channels activated by hyperpolarization in *Arabidopsis thaliana* guard cells (10,57,58). Furthermore, ATP was neither required for cGMP- nor cAMP-activated (49,50) Ca^{2+}-permeable cation channels in many different plant cell types (mesophyll, guard cells or pollen tubes) that also show many of the HACC characteristics. This observation is in contrast to the above-mentioned report where ATP and subsequent protein (de)-phosphorylation was described as a prerequisite for an ABA effect on calcium channels (56). This indicates that there may be more than one subtype of calcium channels co-existing in the PM and/or that additional modes of regulation of these Ca^{2+}-permeable channels are operating which might require ATP- and protein kinases-dependent signaling (56,59).

One discrepancy that stands out in our report is that Mg^{2+} was shown to permeate HACCs in guard cells (10) and in root hairs (51), whereas external Mg^{2+}, in our experiments, did not appear to permeate this channel (Fig. 3A). This is even more intriguing, considering the fact that cGMP was recently shown to activate an inward rectifying current (also Lanthanide-sensitive) with Mg^{2+} as a charge carrier (16). Hence this is another hint that we may be dealing with more than one sub-type of calcium channels. In animal cells, Mn^{2+} was described as both a blocker of Ca^{2+}-channels, if Ca^{2+} is present in the bath, while in the absence of Ca^{2+}, Mn^{2+} permeates the channel (60,61). These data might infer that HACCs, even though sharing many similarities in terms of their biophysical and pharmacological characteristics, might slightly differ from one cell type to another depending on tissue type and/or plant species.

So, the first key finding is that omitting Mg-ATP from the intracellular medium unmasks a larger Gd^{3+}-sensitive non-selective cation conductance that is also regulated by cAMP and ABA. The mechanism consists of shifting the I-V characteristic to the right where less negative voltages can mobilize cations (including Ca^{2+}) through the channel. The second key finding is the demonstration that Mg^{2+} alone can block this conductance (Fig. 6).

The current activated by voltages more negative than -200 mV is small, but significant (Fig. 1A). At the present time, we have no evidence to support that this instantaneous, rectifying and Mg^{2+}-resistant Ba^{2+}-current would be carried by a different population type of HACCs (the channel type unmasked when Mg^{2+} was omitted). If anything, this current could still be carried by the same type of channels since addition of 20 μM Gd^{3+} to the bath is still able to swiftly and efficiently block this current.

In summary, our data describe for the first time that in guard cells, Mg^{2+} blocks I_{Ba} by shifting the I-V relationship and its activation threshold to more negative voltages (Fig. 1C). This effect is reminiscent of the inhibitory effects by Mg^{2+} on many ion-channels that have been interpreted as 'charge screening effects' (18). Indeed, the rectification of the inwardly rectifying K^+ (Kir) channels is due to a voltage-dependent block by cytosolic Mg^{2+} (and polyamines) thereby blocking outward K^+-efflux. Upon hyperpolarization, Mg^{2+} is ejected from the pore, which appears to result in a time-dependent opening of the channel (62,63). Likewise, TRPV6 shows Mg^{2+}-dependent gating that contributes to its strong inward rectification (20) and it was suggested that Mg^{2+} can block the channel by binding to a site within the transmembrane electrical field where it interacts with other permeant cations (20). It is also conceivable that other mechanisms could be operating such as electrostatic interaction between Mg^{2+} and some PM lipids, such as Phosphatidylinositol 4,5-bisphosphate (or PIP_2). It was demonstrated that increasing the amount of membrane PIP_2 results in decreasing the sensitivity of KCNQ channel to inhibition by Mg^{2+} (64). In addition, some Ca^{2+}-channels were found to require PIP_2 for their normal function (65). This begs the question of whether guard cell PM Ca^{2+}-channels are also PIP_2-sensitive. Our results also raise the question of whether Mg^{2+} could be equally important for $I_{K,in}$ gating. Indeed, and unlike earlier reports, we found that activation of $I_{K,in}$ was dependent on Mg^{2+} being present inside the patch pipet (Fig. 6).

Furthermore, the activation of the above HACCs by hyperpolarization and cAMP, the absence of cation selectivity and inhibition by lanthanides is consistent with the hypothesis that channels responsible for the observed effects are CNGCs and this is consistent with our structural modelling that has revealed the presence of di-acidic motifs in the pore forming helix of a subset of AtCNGCs. Acidic residues pointing towards the inner side of the pore, have previously been shown to confer Mg^{2+}-dependence to inward rectifying K^+ channels in animals (47) (Suppl. Fig. 3A). Given the position of the di-acidic motif in the cytoplasmic side of the pore, it is conceivable that Mg^{2+}-binding can be affected by changes in pore opening, for example introduced by cAMP binding to the cytoplasmic region of AtCNGCs. Such a crosstalk would provide a mechanistic explanation for our observation that db_2cAMP overrides the channel blockage produced by 1mM $MgCl_2$ (no added ATP) (Suppl. Fig. 2B).

We therefore propose, firstly, that Mg^{2+} can limit, if not prevent, continuous Ca^{2+}-leakage possibly through all HACCs (including CNGCs) at resting membrane potentials and secondly, that the activation of these channels requires mechanism(s) by which Mg^{2+}-binding is altered, such in the case of adding cAMP (Suppl. Fig. 2B), in turn giving Mg^{2+} an important role in calcium homeostasis and calcium-dependent signaling.

Acknowledgements

This research has been supported by the King Abdullah University of Science and Technology (KAUST). We are indebted to Professor Enid MacRobbie (Department of Plant Science, University of Cambridge, UK) for allowing us to use some of the data gathered by FL-C while in her laboratory (research was supported by BBSRC Grant P05730 to E.M.). We also thank Prof. Mark Tester for his invaluable comments.

Author Contributions

FL-C and CG conceived the study, FL-C performed the experiments and analyzed the data. CG and SA performed the structural analyses. All authors contributed to the writing of the manuscript.

Competing financial interests

The authors declare no competing financial interests.

REFERENCES

1. McAinsh, M. R., and Pittman, J. K. (2009) Shaping the calcium signature. *New Phytol.* **181**, 275-294
2. Véry, A. A., and Sentenac, H. (2002) Cation channels in the *Arabidopsis* plasma membrane. *Trends Plant Sci.* **7**, 168-175
3. White, P. J., and Broadley, M. R. (2003) Calcium in plants. *Ann. Bot.* **92**, 487-511
4. Demidchik, V., Davenport, R. J., and Tester, M. (2002) Nonselective cation channels in plants. *Annu. Rev. Plant Biol.* **53**, 67-107
5. Thion, L., Mazars, C., Nacry, P., Bouchez, D., Moreau, M., Ranjeva, R., and Thuleau, P. (1998) Plasma membrane depolarization-activated calcium channels, stimulated by microtubule-depolymerizing drugs in wild-type *Arabidopsis thaliana* protoplasts, display constitutively large activities and a longer half-life in *ton* 2 mutant cells affected in the organization of cortical microtubules. *Plant J.* **13**, 603-610
6. Miedema, H., Bothwell, J. H., Brownlee, C., and Davies, J. M. (2001) Calcium uptake by plant cells - channels and pumps acting in concert. *Trends Plant Sci.* **6**, 514-519
7. MacRobbie, E. A. C. (1992) Calcium and ABA-induced stomatal closure. *Philos. Trans. Roy. Soc. B.* **338**, 5-18
8. MacRobbie, E. A. C. (2000) ABA activates multiple Ca^{2+} fluxes in stomatal guard cells, triggering vacuolar $K^+(Rb^+)$ release. *Proc. natl. Acad. Sci. U.S.A.* **97**, 12361-12368
9. Hamilton, D. W. A., Hills, A., Köhler, B., and Blatt, M. R. (2000) Ca^{2+} channels at the plasma membrane of stomatal guard cells are activated by hyperpolarization and abscisic acid. *Proc. natl. Acad. Sci. U.S.A.* **97**, 4967-4972
10. Pei, Z. M., Murata, Y., Benning, G., Thomine, S., Klusener, B., Allen, G. J., Grill, E., and Schroeder, J. I. (2000) Calcium channels activated by hydrogen peroxide mediate abscisic acid signalling in guard cells. *Nature* **406**, 731-734
11. Hamilton, D. W. A., Hills, A., and Blatt, M. R. (2001) Extracellular Ba^{2+} and voltage interact to gate Ca^{2+} channels at the plasma membrane of stomatal guard cells. *FEBS Lett.* **491**, 99-103
12. Leng, Q., Mercier, R. W., Yao, W., and Berkowitz, G. A. (1999) Cloning and first functional characterization of a plant cyclic nucleotide-gated cation channel. *Plant Physiol.* **121**, 753-761
13. Leng, Q., Mercier, R. W., Hua, B. G., Fromm, H., and Berkowitz, G. A. (2002) Electrophysiological analysis of cloned cyclic nucleotide-gated ion channels. *Plant Physiol.* **128**, 400-410
14. Balagué, C., Lin, B. Q., Alcon, C., Flottes, G., Malmstrom, S., Köhler, C., Neuhaus, G., Pelletier, G., Gaymard, F., and Roby, D. (2003) HLM1, an essential signaling component in the hypersensitive response, is a member of the cyclic nucleotide-gated channel ion channel family. *Plant Cell* **15**, 365-379
15. Lemtiri-Chlieh, F., and Berkowitz, G. A. (2004) Cyclic adenosine monophosphate regulates calcium channels in the plasma membrane of Arabidopsis leaf guard and mesophyll cells. *J. Biol. Chem.* **279**, 35306-35312
16. Wang, Y. F., Munemasa, S., Nishimura, N., Ren, H. M., Robert, N., Han, M., Puzorjova, I., Kollist, H., Lee, S., Mori, I., and Schroeder, J. I. (2013) Identification of cyclic GMP-activated

nonselective Ca^{2+}-permeable cation channels and associated CNGC5 and CNGC6 genes in Arabidopsis Guard Cells. *Plant Physiol.* **163**, 578-590

17. Wu, J. Y., Qu, H. Y., Jin, C., Shang, Z. L., Wu, J., Xu, G. H., Gao, Y. B., and Zhang, S. L. (2011) cAMP activates hyperpolarization-activated Ca^{2+}-channels in the pollen of *Pyrus pyrifolia*. *Plant Cell Rep.* **30**, 1193-1200
18. Hille, B. (2001) *Ion channels of excitable membranes*, 3rd ed., Sinauer Associates, Inc, Sunderland, MA
19. Matsuda, H. (1988) Open-state substructure of inwardly rectifying potassium channels revealed by magnesium block in guinea-pig heart-cells. *J. Physiol.* **397**, 237-25820
20. Voets, T., Janssens, A., Prenen, J., Droogmans, G., and Nilius, B. (2003) Mg^{2+}-dependent gating and strong inward rectification of the cation channel TRPV6. *J. Gen. Physiol.* **121**, 245-260
21. Zito, K., and Scheuss, V. (2009) NMDA Receptor Function and Physiological Modulation. in *Encyclopedia of Neuroscience* (Squire, L. R. ed.), Academic Press, Oxford
22. Nowak, L. M., Ascher, P., Bregestovski, P., Herbet, A., and Prochiantz, A. (1984) Voltage dependence of 1-Glu induced current is due to gating by Mg ions. *Biophys. J.* **45**, A388-A388
23. Schroeder, J. I. (1995) Magnesium-independent activation of inward-rectifying K^+ channels in *Vicia-faba* guard-cells. *FEBS Lett.* **363**, 157-160
24. Hedrich, R., Moran, O., Conti, F., Busch, H., Becker, D., Gambale, F., Dreyer, I., Kuch, A., Neuwinger, K., and Palme, K. (1995) Inward rectifier potassium channels in plants differ from their animal counterparts in response to voltage and channel modulators. *Eur. Biophys. J.* **24**, 107-115
25. Pei, Z. M., Ward, J. M., and Schroeder, J. I. (1999) Magnesium sensitizes slow vacuolar channels to physiological cytosolic calcium and inhibits fast vacuolar channels in fava bean guard cell vacuoles. *Plant Physiol.* **121**, 977-986
26. Bruggemann, L. I., Pottosin, I. I., and Schönknecht, G. (1999) Cytoplasmic magnesium regulates the fast activating vacuolar cation channel. *J. Exp. Bot.* **50**, 1547-1552
27. Carpaneto, A., Cantu, A. M., and Gambale, F. (2001) Effects of cytoplasmic Mg^{2+} on slowly activating channels in isolated vacuoles of *Beta vulgaris*. *Planta* **213**, 457-468
28. Pottosin, I., Martinez-Estevez, M., Dobrovinskaya, O., Muniz, J., and Schönknecht, G. (2004) Mechanism of luminal Ca^{2+} and Mg^{2+} action on the vacuolar slowly activating channels. *Planta* **219**, 1057-1070
29. Wolf, T., Guinot, D. R., Hedrich, R., Dietrich, P., and Marten, I. (2005) Nucleotides and Mg^{2+} ions differentially regulate K^+ channels and non-selective cation channels present in cells forming the stomatal complex. *Plant Cell Physiol.* **46**, 1682-1689
30. Tyerman, S. D., Whitehead, L. F., and Day, D. A. (1995) A channel-like transporter for NH_4^+ on the symbiotic interface of N_2-fixing plants. *Nature* **378**, 629-632
31. Obermeyer, G., and Tyerman, S. D. (2005) NH_4^+ currents across the peribacteroid membrane of soybean. Macroscopic and microscopic properties, inhibition by Mg^{2+}, and temperature dependence indicate a subpicosiemens channel finely regulated by divalent cations. *Plant Physiol.* **139**, 1015-1029
32. Babenko, A. P., Aguilar-Bryan, L., and Bryan, J. (1998) A view of $SUR/K_{IR}6.X$, K_{ATP} channels. *Annu. Rev. Physiol.* **60**, 667-687
33. Campbell, J. D., Sansom, M. S. P., and Ashcroft, F. M. (2003) Potassium channel regulation - Structural insights into the function of the nucleotide-binding domains of the human sulphonylurea receptor. *EMBO Rep.* **4**, 1038-1042
34. Assmann, S. M., Simoncini, L., and Schroeder, J. I. (1985) Blue-light activates electrogenic ion pumping in guard-cell protoplasts of *Vicia faba*. *Nature* **318**, 285-287
35. Schroeder, J. I. (1988) K^+ Transport-Properties of K^+ Channels in the Plasma-Membrane of Vicia-Faba Guard-Cells. *J. Gen. Physiol.* **92**, 667-683

36. Blatt, M. R. (1987) Electrical characteristics of stomatal guard-cells - the ionic basis of the membrane-potential and the consequence of KCl leakage from microelectrodes. *Planta* **170**, 272-287
37. Lemtiri-Chlieh, F. (1996) Effects of internal K^+ and ABA on the voltage- and time-dependence of the outward K^+-rectifier in *Vicia* guard cells. *J. Memb. Biol.* **153**, 105-116
38. Lemtiri-Chlieh, F., and Macrobbie, E. A. C. (1994) Role of calcium in the modulation of *Vicia* guard-cell potassium channels by abscisic acid: a patch-clamp study. *J. Memb. Biol.* **137**, 99-107
39. Neher, E. (1992) Correction for liquid junction potentials in patch clamp experiments. *Methods Enzymol.* **207**, 123-131
40. Shaff, J. E., Schultz, B. A., Craft, E. J., Clark, R. T., and Kochian, L. V. (2010) GEOCHEM-EZ: a chemical speciation program with greater power and flexibility. *Plant Soil* **330**, 207-214
41. Ishida, T., and Kinoshita, K. (2008) Prediction of disordered regions in proteins based on the meta approach. *Bioinformatics* **24**, 1344-1348
42. Buchan, D. W., Minneci, F., Nugent, T. C., Bryson, K., and Jones, D. T. (2013) Scalable web services for the PSIPRED Protein Analysis Workbench. *Nucleic Acids Res.* **41**, W349-357
43. Edgar, R. C. (2004) MUSCLE: a multiple sequence alignment method with reduced time and space complexity. *BMC Bioinformatics.* **5**, 113
44. Blatt, M. R. (1992) K^+ channels of stomatal guard-cells - characteristics of the inward rectifier and its control by pH. *J. Gen. Physiol.* **99**, 615-644
45. Zagotta, W. N., and Siegelbaum, S. A. (1996) Structure and function of cyclic nucleotide-gated channels. *Ann. Rev. Neurosci.* **19**, 235-263
46. Tao, X., Avalos, J. L., Chen, J., and MacKinnon, R. (2009) Crystal structure of the eukaryotic strong inward-rectifier K^+ channel Kir2.2 at 3.1 Å resolution. *Science* **326**, 1668-1674
47. Zelman, A. K., Dawe, A., Gehring, C., and Berkowitz, G. A. (2012) Evolutionary and structural perspectives of plant cyclic nucleotide-gated cation channels. *Front. Plant Sci.* **3**, 95
48. Clayton, G. M., Altieri, S., Heginbotham, L., Unger, V. M., and Morais-Cabral, J. H. (2008) Structure of the transmembrane regions of a bacterial cyclic nucleotide-regulated channel. *Proc. natl. Acad. Sci. U.S.A.* **105**, 1511-1515
49. Hua, B. G., Mercier, R. W., Leng, Q., and Berkowitz, G. A. (2003) Plants do it differently. A new basis for potassium/sodium selectivity in the pore of an ion channel. *Plant Physiol.* **132**, 1353-1361
50. Bush, D. S., Hedrich, R., Schroeder, J. I., and Jones, R. L. (1988) Channel-mediated K^+ flux in barley aleurone protoplasts. *Planta* **176**, 368-377
51. Véry, A. A., and Davies, J. M. (2000) Hyperpolarization-activated calcium channels at the tip of *Arabidopsis* root hairs. *Proc. natl. Acad. Sci. U.S.A.* **97**, 9801-9806
52. Miedema, H., Demidchik, V., Very, A. A., Bothwell, J. H. F., Brownlee, C., and Davies, J. M. (2008) Two voltage-dependent calcium channels co-exist in the apical plasma membrane of *Arabidopsis thaliana* root hairs. *New Phytol.* **179**, 378-385
53. Murata, Y., Pei, Z. M., Mori, I. C., and Schroeder, J. (2001) Abscisic acid activation of plasma membrane Ca^{2+} channels in guard cells requires cytosolic NAD(P)H and is differentially disrupted upstream and downstream of reactive oxygen species production in *abi1-1* and *abi2-1* protein phosphatase 2C mutants. *Plant Cell* **13**, 2513-2523
54. Demidchik, V., Bowen, H. C., Maathuis, F. J. M., Shabala, S. N., Tester, M. A., White, P. J., and Davies, J. M. (2002) *Arabidopsis thaliana* root non-selective cation channels mediate calcium uptake and are involved in growth. *Plant J.* **32**, 799-808
55. Lemtiri-Chlieh, F., MacRobbie, E. A. C., Webb, A. A. R., Manison, N. F., Brownlee, C., Skepper, J. N., Chen, J., Prestwich, G. D., and Brearley, C. A. (2003) Inositol hexakisphosphate mobilizes an endomembrane store of calcium in guard cells. *Proc. natl. Acad. Sci. U.S.A.* **100**, 10091-10095
56. Köhler, B., and Blatt, M. R. (2002) Protein phosphorylation activates the guard cell Ca^{2+} channel and is a prerequisite for gating by abscisic acid. *Plant J.* **32**, 185-194

57. Munemasa, S., Oda, K., Watanabe-Sugimoto, M., Nakamura, Y., Shimoishi, Y., and Murata, Y. (2007) The coronatine-insensitive 1 mutation reveals the hormonal signaling interaction between abscisic acid and methyl jasmonate in arabidopsis guard cells. Specific impairment of ion channel activation and second messenger production. *Plant Physiol.* **143**, 1398-1407
58. Vahisalu, T., Kollist, H., Wang, Y. F., Nishimura, N., Chan, W. Y., Valerio, G., Lamminmaki, A., Brosche, M., Moldau, H., Desikan, R., Schroeder, J. I., and Kangasjarvi, J. (2008) SLAC1 is required for plant guard cell S-type anion channel function in stomatal signalling. *Nature* **452**, 487-491
59. Mori, I. C., Murata, Y., Yang, Y., Munemasa, S., Wang, Y. F., Andreoli, S., Tiriac, H., Alonso, J. M., Harper, J. F., Ecker, J. R., Kwak, J. M., and Schroeder, J. I. (2006) CDPKs CPK6 and CPK3 function in ABA regulation of guard cell S-type anion- and Ca^{2+}-permeable channels and stomatal closure. *PLoS Biol.* **4**, e327
60. Coraboeuf, E. (1980) Voltage clamp studies of the slow inward current. in *The slow inward current and cardiac arrhythmias*, 1st Ed., Martinus Nijhoff, The Hague. pp25-95
61. Bannister, R. A., Pessah, I. N., and Beam, K. G. (2009) The skeletal L-type Ca^{2+} current is a major contributor to excitation-coupled Ca^{2+} entry. *J Gen. Physiol.* **133**, 79-91
62. Nichols, C. G., and Lopatin, A. N. (1997) Inward rectifier potassium channels. *Annu. Rev. Physiol.* **59**, 171-191
63. Guo, D. L., Ramu, Y., Klem, A. M., and Lu, Z. (2003) Mechanism of rectification in inward-rectifier K^+ channels. *J Gen. Physiol.* **121**, 261-275
64. Suh, B. C., and Hille, B. (2007) Electrostatic interaction of internal Mg^{2+} with membrane PIP_2 seen with KCNQ K^+ channels. *J. Gen. Physiol.* **130**, 241-256
65. Gamper, N., Reznikov, V., Yamada, Y., Yang, J., and Shapiro, M. S. (2004) Phosphotidylinositol 4,5-bisphosphate signals underlie receptor-specific $G_{q/11}$-mediated modulation of N-type Ca^{2+} channels. *J. Neurosci.* **24**, 10980-10992

Figure 1

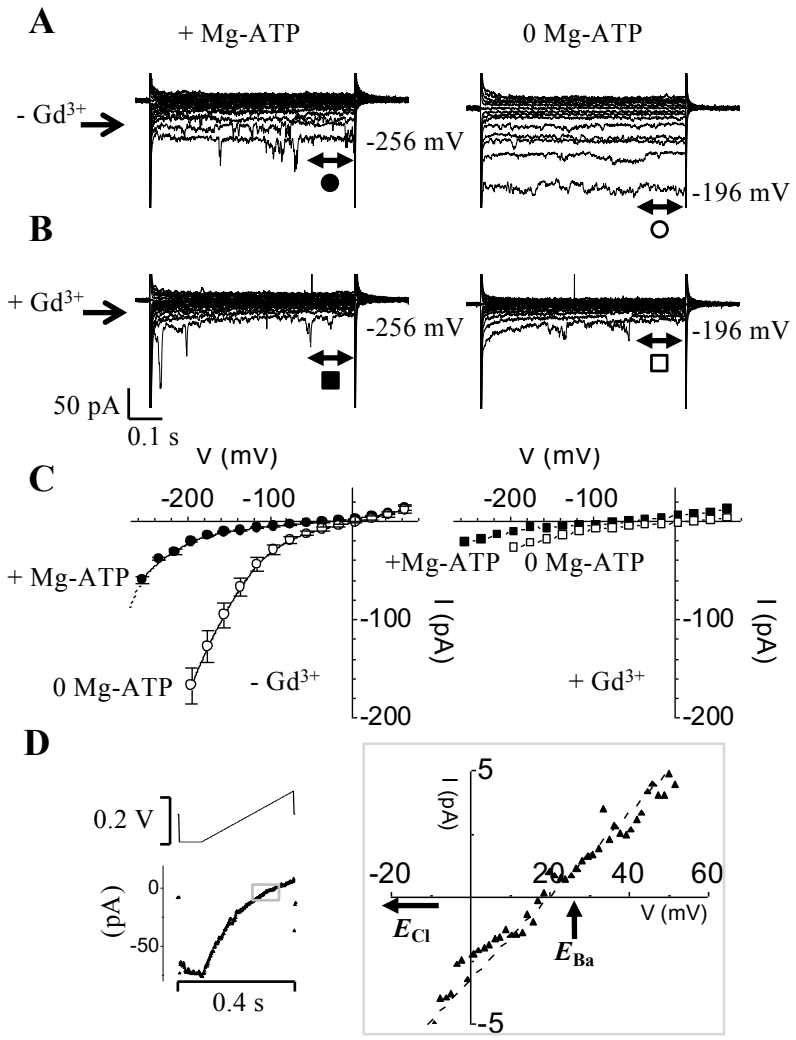

Figure 1. **Removal of intracellular Mg-ATP unveils a larger instantaneously-activated, inwardly-directed and Gd^{3+}-sensitive Ba^{2+} current**. (**A**) Typical examples of current traces in whole-cell mode obtained from two separate guard cells with the pipette solution either containing (*left traces*) or lacking (*right traces*) Mg-ATP (1 mM). The pulse protocol mostly used throughout this study consists of 0.6 s long square voltage pulses ranging from +64 to -256 mV in -20 mV increments; the holding potential h_v was set to -36 mV. In order to preserve the quality of the 'Giga' seals, GCPs with no Mg-ATP in the pipette were not subjected to higher voltages beyond -196 mV. (**B**) Current traces of I_{Ba} obtained from the same cells and in the same conditions as described in (A) except for the external solution containing Gd^{3+} (20 µM; left or 100 µM; right) (**C**) Current-voltage relationships (I-V); *left panel*: superimposed I-Vs of I_{Ba} in the absence (○; n=7) or presence (●: n=3) of Mg-ATP. *Right panel*: I-V relations in the presence of Gd^{3+} (■: +Mg-ATP; □: -Mg-ATP). (**D**) Typical current trace recorded in the absence of Mg-ATP (below) in response to the 'E_{rev} protocol' which consists of activating I_{Ba} using a hyperpolarization square pulse to -156 mV and immediately followed by a continuous depolarizing ramp to +64 mV (the voltage protocol is depicted above) with a slope of 0.7 V s^{-1}. Scale bars are shown below the current traces and to the left of the voltage protocol.

Figure 2

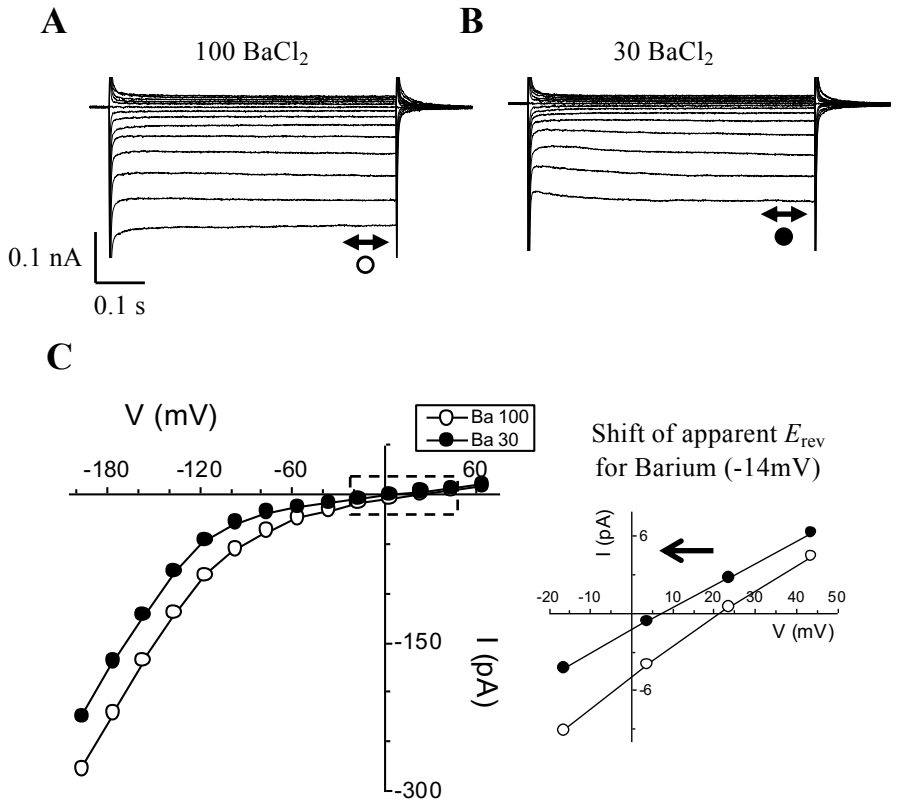

Figure 2. **Decreasing $[Ba^{2+}]_o$ from 100 to 30 mM not only decreases the hyperpolarization-activated I_{Ba} but also shifts its apparent E_{rev} (~- 14 mV)**. (**A**) and (**B**) Typical current traces of hyperpolarization-activated I_{Ba} recorded from the same guard cell either in 100 (A) or 30 mM (B) $[Ba^{2+}]_o$. Scale bars are shown below the current traces. (**C**) Corresponding I-V plots of I_{Ba} in 100 and 30 mM $[Ba^{2+}]_o$ taken from the current traces shown in (A) and (B). Inset: Zoomed I-V plot from the the area shown as a dashed box in (C). The inset shows the amount (in mV) and the direction (arrow) of the shift in the apparent E_{rev} when the bath perfusion was switched from 100 to 30 mM Ba^{2+}.

Figure 3

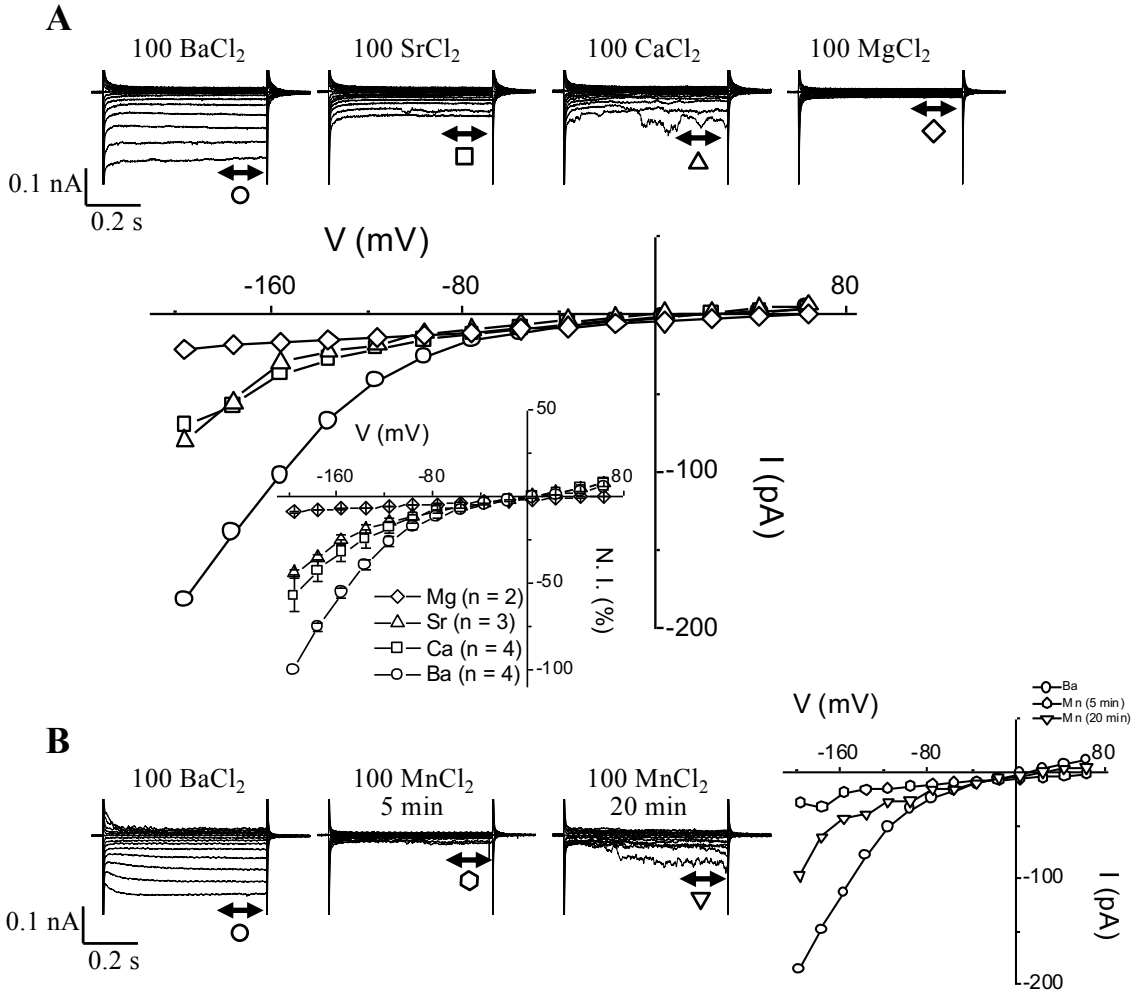

Figure 3. **Current through I_{Ba} channels can be carried by other divalent cations such as Ca^{2+}, Sr^{2+} and even Mn^{2+} but not by Mg^{2+}.** (**A**) Typical current traces and corresponding I-V plots recorded in the presence of 100 mM $BaCl_2$, 100 mM $CaCl_2$, 100 mM $SrCl_2$ and 100 mM $MgCl_2$ (note that all traces are from the same guard cell except for $MgCl_2$). Inset: Normalized group I-V curves showing divalent permeabilities (the mean current values obtained for Ca^{2+}, Sr^{2+} and Mg^{2+} were normalized to the mean current value obtained in Ba^{2+} at -196 mV). (**B**) Typical current traces and corresponding I-V plots recorded in the presence of 100 mM $BaCl_2$ and 100 $MnCl_2$ at times 5 and 20 minutes. All traces are from the same guard cell. Notice the transient blocking effect of Mn^{2+} ions.

Figure 4

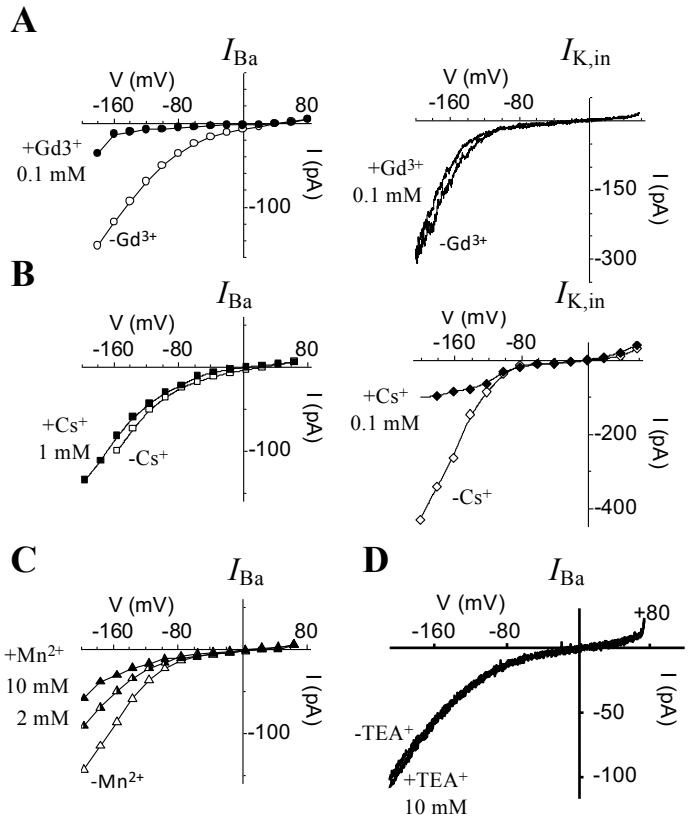

Figure 4. **Differential effects of some known blockers on the two main PM conductances activated by hyperpolarization in guard cells: namely, I_{Ba} and $I_{K,in}$**. (**A**) I-V plots showing the effect of Gd^{3+} (0.1 mM) on I_{Ba} (*left panel*) and $I_{K,in}$ (*right panel*). (**B**) I-V plots showing the effect of 1 mM Cs^+ on I_{Ba} (*left panel*) compared to the effect of 0.1 mM Cs^+ on $I_{K,in}$ (*right panel*). (**C**) I-V plot showing the effect of Mn^{2+} on I_{Ba} recorded from the same GCP using 2 and 10 mM in the bath. (**D**) I_{Ba}-V plots generated from current recordings using hyperpolarizing ramps (+64 to -196 mV; 0.7 $V.s^{-1}$; h_v = -36 mV) showing the effect of 10 mM TEA^+ added to the bath.

Figure 5

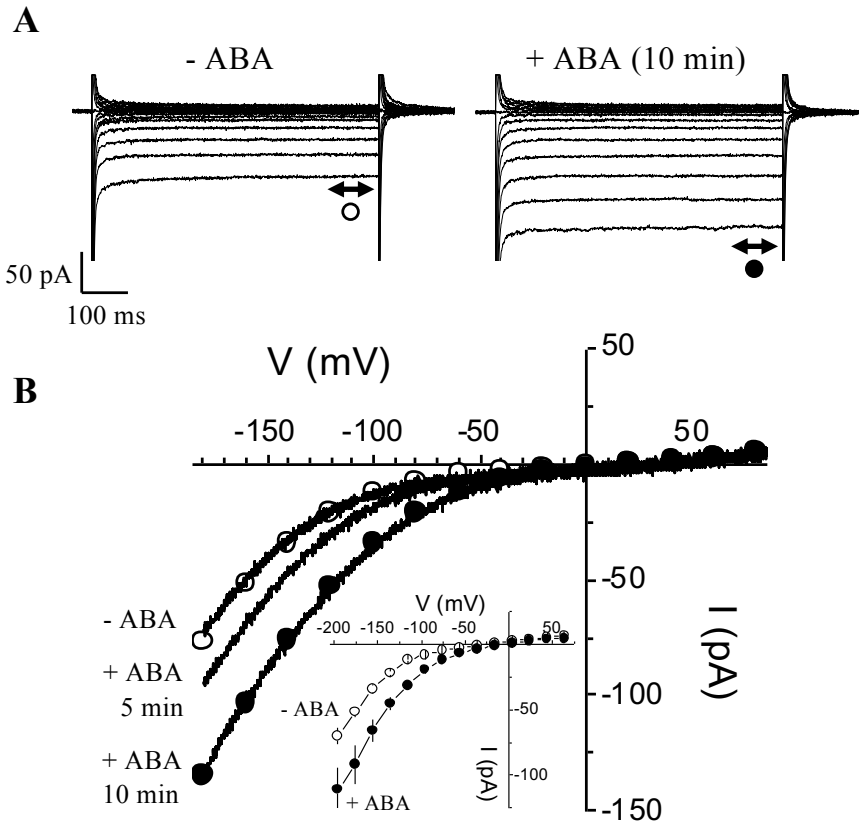

Figure 5. **Rapid enhancement of I_{Ba} by ABA**. (**A**) I_{Ba} currents in the absence of Mg-ATP in the patch pipet recorded from the same guard cell in response to hyperpolarizing voltages (from +64 to -196 mV; in -20 mV increments) before (○) and 10 minutes after (●) bath application of ABA (20 mM). (**B**) I-V plots of the effect of ABA showing the enhancing effect of ABA with time. (control: -ABA; 5 and 10 minutes after continuous bath perfusion with ABA). We also superimposed the measurements generated by voltage ramps for the control and 10 min ABA. Inset: Superimposed I-V plots showing the average effect of ABA on I_{Ba} (0 Mg-ATP). Data are current average measurements (± sem) from different experiments (n=3) before (○) and about 10 minutes after (●) bath perfusion with ABA (Student test; *: P≤0.05, **: P≤0.01, ns: P> 0.05).

Figure 6

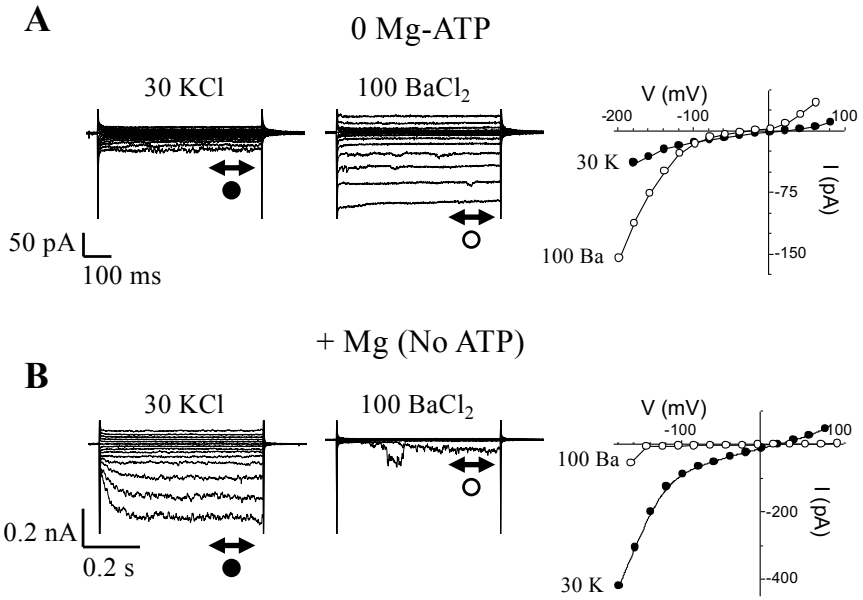

Figure 6. **Internal Mg^{2+} is responsible for I_{Ba} inhibition**. (**A**) Currents (*left panel*) and corresponding I-V plots (*right panel*) from the same guard cell recorded in response to hyperpolarizing voltage steps (from +64 to -196 mV; in -20 mV increments; h_v = -36 mV) and in the absence of Mg-ATP either using K^+ (30 mM) or Ba^{2+} (100 mM) as charge carriers. Notice the larger I_{Ba} compared to $I_{K,in}$. (**B**) Current (*left panel*) and corresponding I-V relationships (*right panel*) recorded in the same external conditions as in (A) but this time, using only Mg^{2+} ions in the patch solution (1 mM added as $MgCl_2$) and no added ATP. In these conditions, the predominant current activated by hyperpolarization is $I_{K,in}$, not I_{Ba}.

Figure 7

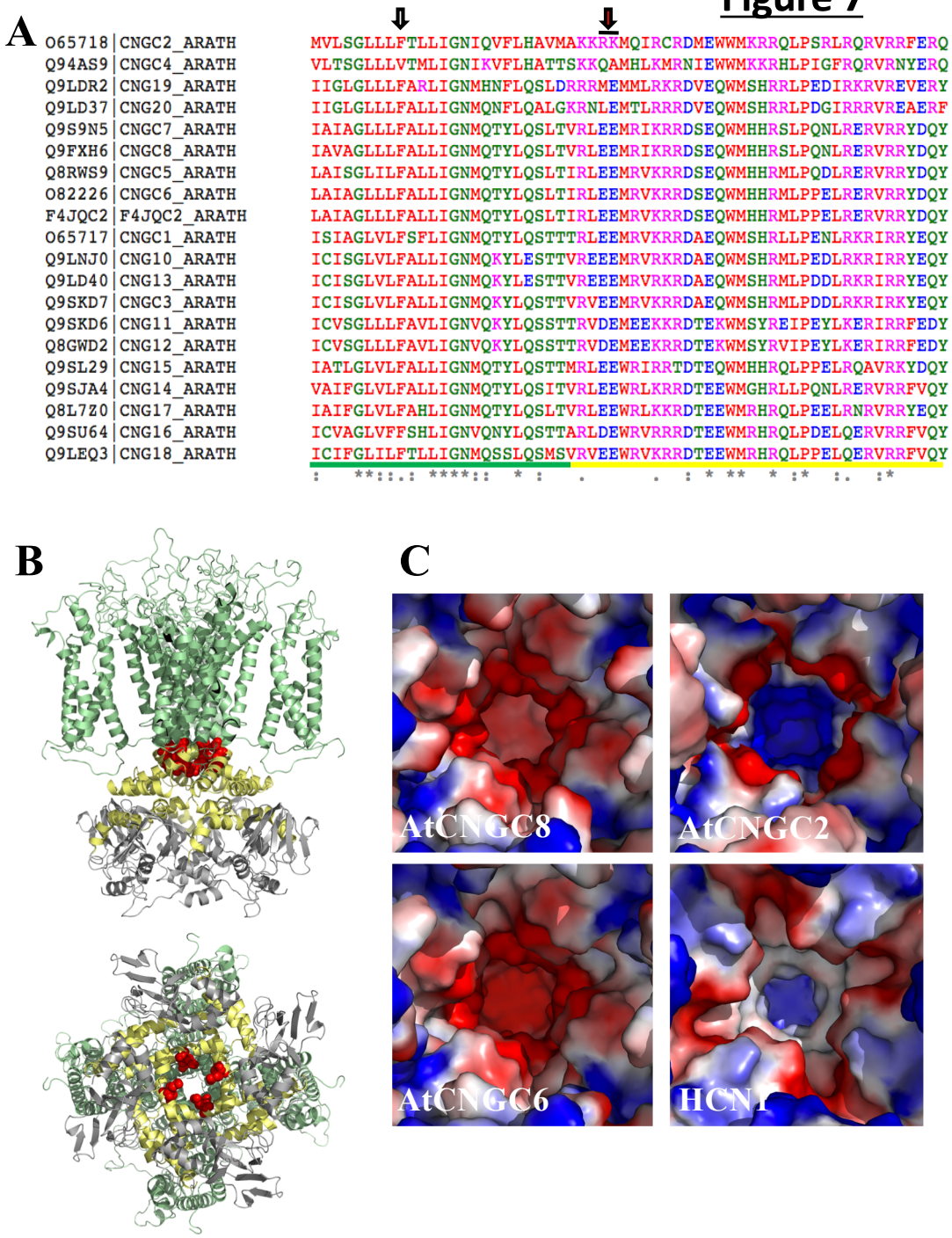

Figure 7. Structural rationale for the channel-blocking effect of Mg^{2+}. (**A**) Sequence alignment of the AtCNGC protein sequence surrounding the putative Mg^{2+} binding site. The di-acidic motif present in most AtCNGCs is highlighted by a red arrow and black line, whereas the location corresponding to the Mg^{2+}-binding acidic motif in the Kir2.2 pore domain is indicated by the left arrow (grey filling). The residues of the pore and linker regions are underlined green and yellow, respectively. (**B**) Structural model of AtCNGC8, based on human HCN1 (PDB accession number 5u6o). *Top panel*: side view, with the transmembrane region coloured in green, the linker region in yellow, and the cytoplasmic cAMP binding domain in grey. The di-acidic motif (residues E437 and E438 in AtCNGC8) are highlighted as red sphere models. *Bottom panel*: view from the cytoplasm into the channel (90˚ rotation with respect to top panel). (**C**) Electro-static surface representation (colour-ramped from negatively charged, red, to positively charged, blue) of homology models of AtCNGCs containing the di-acidic motif (AtCNGC8 and 6) and of AtCNGC2 (model) and human HCN1 (PDB 5u6o) lacking this motif.

Suppl. Figure 1

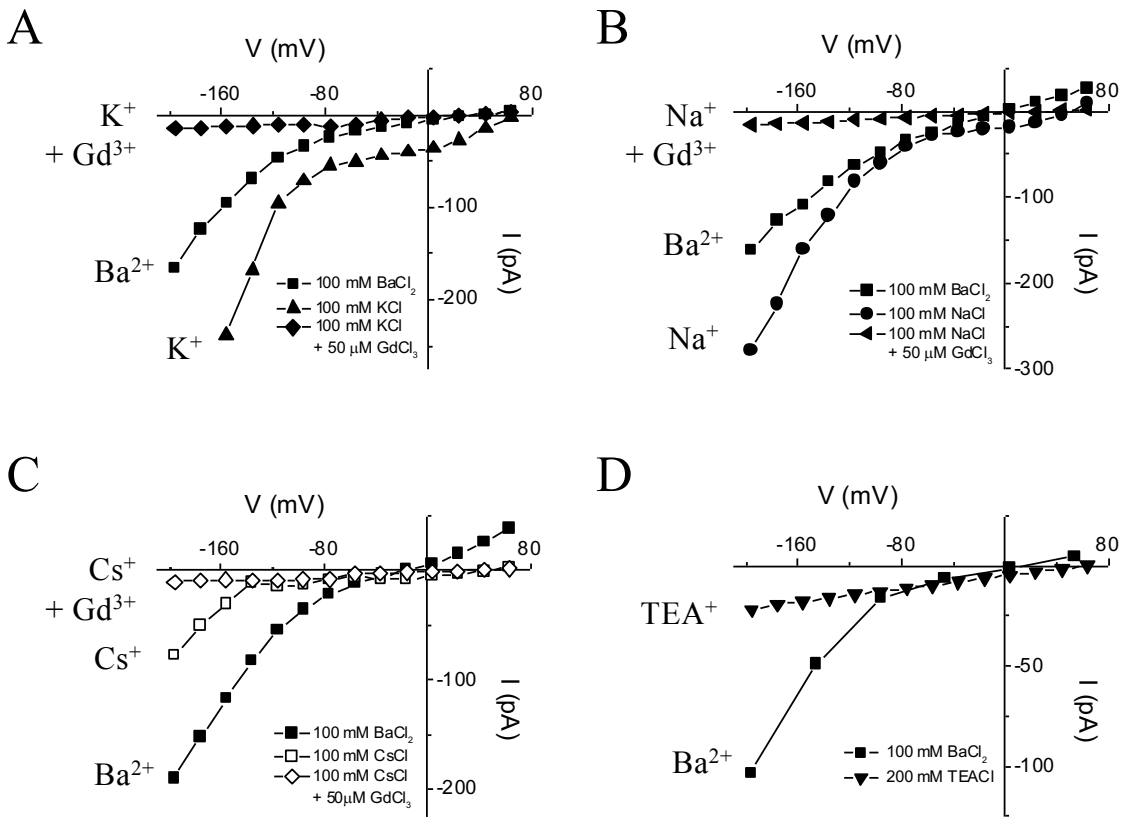

In the absence of MgATP, Guard cell's HACCs are permeable to monovalent cations such as K^+, Na^+, Cs^+ but not TEA^+. All experiments were conducted in the whole cell configuration where *V. faba* GCPs were held at -56 mV. (**A**) Superimposed I-V plots in the presence of 100 mM $BaCl_2$ (■), 100 mM KCl (▲) or 100 KCl + 0.05 mM $GdCl_3$. (**B**) Superimposed I-V plots in the presence of 100 mM $BaCl_2$ (■), 100 mM NaCl (●) or 100 NaCl + 0.05 mM $GdCl_3$. (**C**) Superimposed I-V plots in the presence of 100 mM $BaCl_2$ (■) or 100 mM CsCl (□) or 100 CsCl + 0.05 mM $GdCl_3$ (◇). (**D**) Superimposed I-V plots in the presence of 100 mM $BaCl_2$ (■) or 100 TEACl (▼).

Suppl. Figure 2

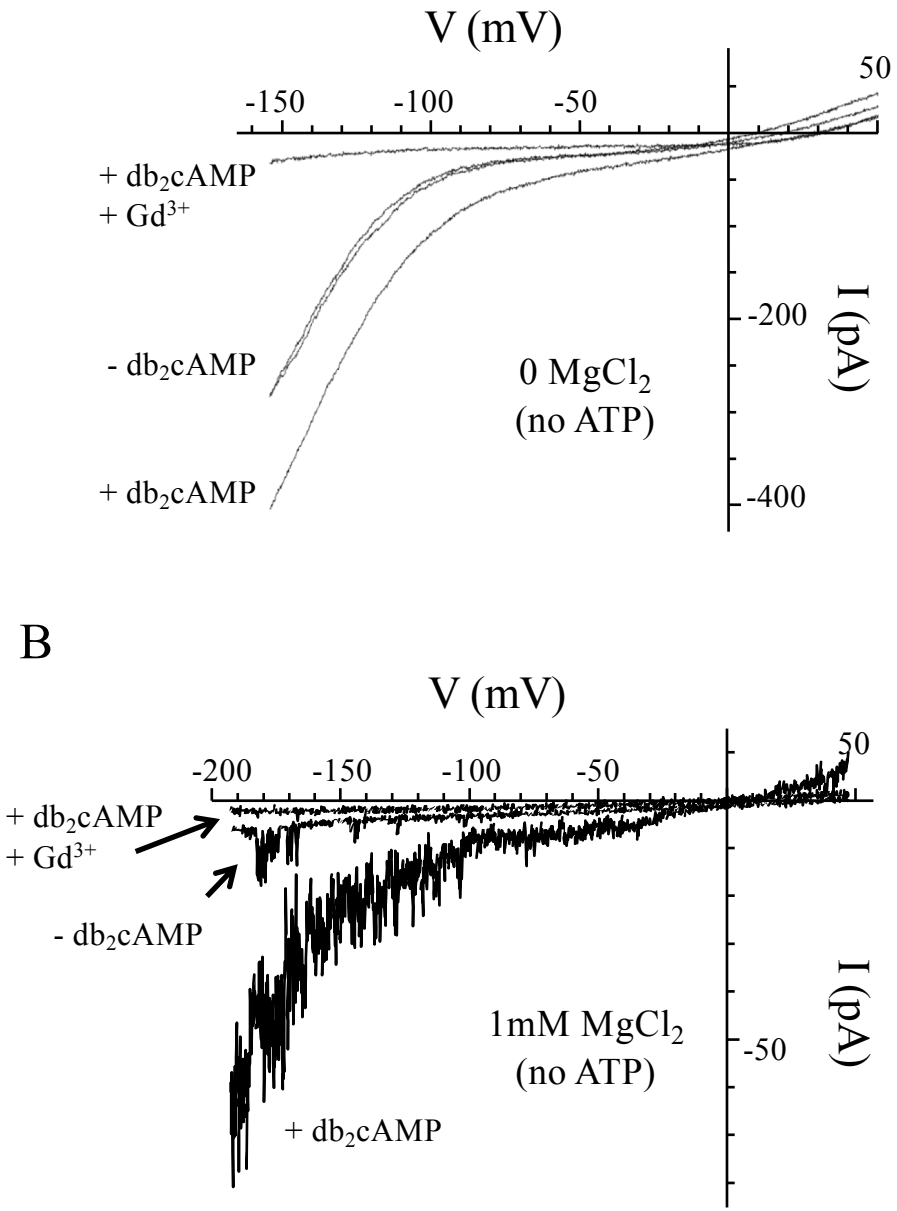

Dibutyryl cyclic AMP potentiates a Gd^{3+}-sensitive current in guard cells either in the presence or absence of intracellular Mg^{2+}. Experiments were conducted in the whole cell configuration where the GCPs were held at -52 mV and the I-V plots were generated using a hyperpolarizing ramp protocol. see Methods for bath and intracellular media. (**A**) Typical example from a *V. faba* GCP patched with no MgATP in the intracellular media showing superimposed I-V ramps from +50 to -156 mV (70 $mV.s^{-1}$) in the absence (- db_2cAMP) or presence (+ db_2cAMP) of 1 mM dibutyryl cyclic AMP. Note that adding 0.05 mM $GdCl_3$ while keeping db_2cAMP in the bath blocks this conductance. (**B**) Typical example from an *A. thaliana* GCP patched with 1mM $MgCl_2$ (no added ATP) in the intracellular media showing superimposed I-V ramps from ~50 to -192 mV (70 $mV.s^{-1}$) in the absence (- db_2cAMP) or presence (+ db_2cAMP) of 1 mM dibutyryl cyclic AMP. Note that adding 0.05 mM $GdCl_3$ while keeping db_2cAMP in the bath also blocks this conductance.

Suppl. Figure 3

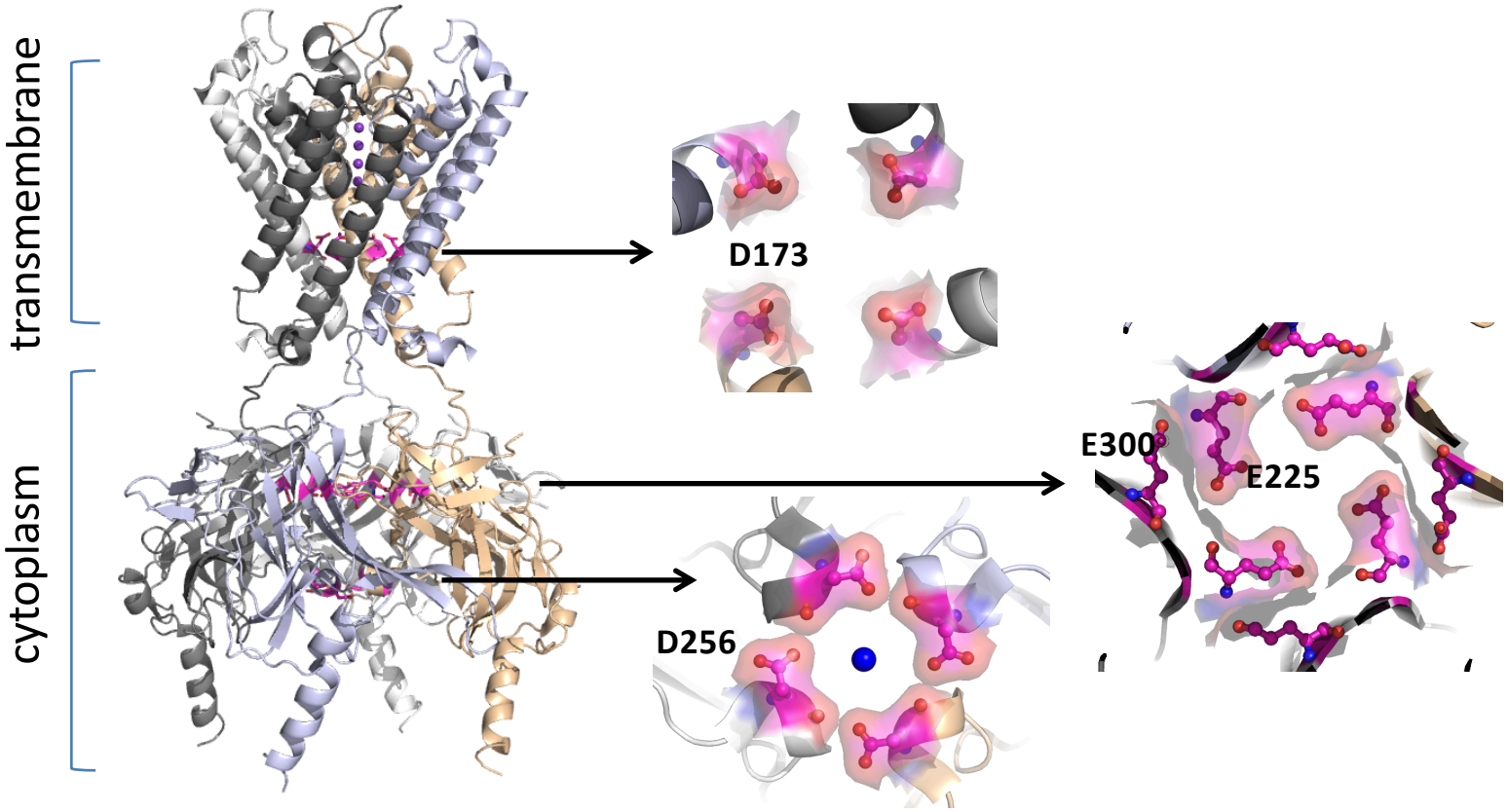

Mechanism of inward rectifying by magnesium ions. Tao *et al*. (Science 2009, 326, 1668-1674) have shown that inward rectifying through Mg^{2+} can be explained by the ion binding to negatively charged regions in the pore (formed by D173) and in the cytoplasmic regulatory domains (D256 and E300/E225). The crystal structure of the inward rectifying potassium channel Kir2.2 (Tao, 2009; PDB entry 3JYC) is shown in ribbon presentation. The four subunits are colour-coded. Potassium ions in the channel are shown as magenta spheres. Negatively charged residues that bind the Mg^{2+} - mimic Sr^{2+} in the crystal structure are shown in pink in their molecular surface.